Journal of Controlled Release 224 (2016) 229–238

Contents lists available at ScienceDirect

Journal of Controlled Release

journal homepage: www.elsevier.com/locate/jconrel

Findings questioning the involvement of Sigma-1 receptor in the uptake of anisamide-decorated particles

Athanasia Dasargyri [1], Pablo Hervella [1,2], Ailsa Christiansen, Steven T. Proulx, Michael Detmar, Jean-Christophe Leroux *

Department of Chemistry and Applied Biosciences, Institute of Pharmaceutical Sciences, Swiss Federal Institute of Technology Zurich (ETHZ), Zurich 8093, Switzerland

ARTICLE INFO

Article history:
Received 14 August 2015
Received in revised form 9 January 2016
Accepted 11 January 2016
Available online 13 January 2016

Keywords:
Anisamide
Sigma-1 receptor
Receptor-mediated endocytosis
Drug targeting

ABSTRACT

Anisamide is a small benzamide previously suggested as a tumor-targeting ligand for nanocarriers and it has been shown to enhance tumor uptake *in vitro* as well as *in vivo* when grafted on the nanoparticle surface. Anisamide has been hypothesized to interact with the Sigma-1 receptor, based on the binding of larger benzamides, which contain anisamide in their structure, to this receptor. However, the interaction between anisamide and Sigma-1 receptor has never been thoroughly studied. We developed fluorescent PEGylated particles decorated with anisamide, which were preferentially taken up *in vitro* by melanoma cells compared to macrophages. The anisamide-decorated particles were used to study their interaction with the Sigma-1 receptor. The absence of competition of Sigma-1 receptor ligands for the particle uptake was a first indication that the receptor might not be involved in the uptake process. In addition, the extent of particle uptake did not correlate with the levels of cellular expression of Sigma-1 receptor in the cell models tested. Immunostaining of the receptor on melanoma cells revealed intracellular localization, indirectly excluding the possibility of anisamide binding to the receptor when grafted on the particles. All these data question the previously suggested Sigma-1 receptor-mediated uptake of the anisamide-decorated particles, a finding which may have an impact on the use of anisamide as a targeting ligand.

© 2016 Elsevier B.V. All rights reserved.

1. Introduction

Despite the fact that researchers are still far from developing ideal cancer chemotherapeutics, recent advances in molecular cancer biology and a better understanding of tumor heterogeneity have enabled significant progress towards targeted tumor therapy [1]. Equally important to this process have been improvements in the design and characterization of various classes of tumor-directed delivery systems for drugs and imaging agents [2]. Among them, particle-based delivery systems have played a dominant role in the scientific literature in the last decades, although the clinical output has so far been limited [3,4]. As a strategy to increase the benefits from the preferential tumor accumulation of colloids following intravenous (i.v.) injection, researchers have focused on decorating nanoparticles with affinity ligands that are able to recognize cell-surface antigens unique for or overexpressed by cancer cells [5,6]. This strategy aims to increase the interaction between tumor cells and carriers once the latter have reached the tumor tissue. This interaction could potentially lead to prolonged residence time of the carriers in the tumor tissue and/or result in enhanced internalization by tumor cells, consequently leading to higher anti-tumor efficacy [7].

Molecules currently evaluated in preclinical research as tumor-targeting ligands for particulate systems can be classified into two major categories according to their nature: biologic macromolecules and small molecules. Large biological molecules (*e.g.* antibodies or other proteins) or small biologics (antibody fragments, peptides, aptamers) excel in binding affinity and specificity for tumor antigens. However, small molecules, such as mono- or disaccharides, biotin or folic acid, although generally less affine, present numerous advantages as tumor-targeting moieties of particles, including lower risk of immunogenicity, higher stability in the blood circulation, reduced cost of production and ease of incorporation on the surface of particle carrier systems by means of simple chemistry [6,8]. Folic acid [9] and *S,S*-2-[3-[5-amino-1-carboxypentyl]-ureido]-pentanedioic acid [10] constitute encouraging examples of small ligands that are now under thorough investigation for their tumor-targeting potential. Another small molecule which has been proposed as a tumor-directing moiety for the decoration of nanocarriers is the 4-methoxybenzamide derivative named anisamide (Fig. 1A).

The concept of using anisamide as a tumor-targeting moiety for nanocarriers was first proposed by Huang and colleagues in 2004 [11]. It was inspired by a class of benzamide-based compounds with cancer selective properties. In fact, radiolabeled iodobenzamide molecules

* Corresponding author.
E-mail address: jleroux@ethz.ch (J.-C. Leroux).
[1] A. Dasargyri and P. Hervella contributed equally to this work.
[2] Current address: Center for Single Particle Science and Engineering, Department of Physics, Chemistry and Pharmacy, University of Southern Denmark, Odense, Denmark.

http://dx.doi.org/10.1016/j.jconrel.2016.01.021
0168-3659/© 2016 Elsevier B.V. All rights reserved.

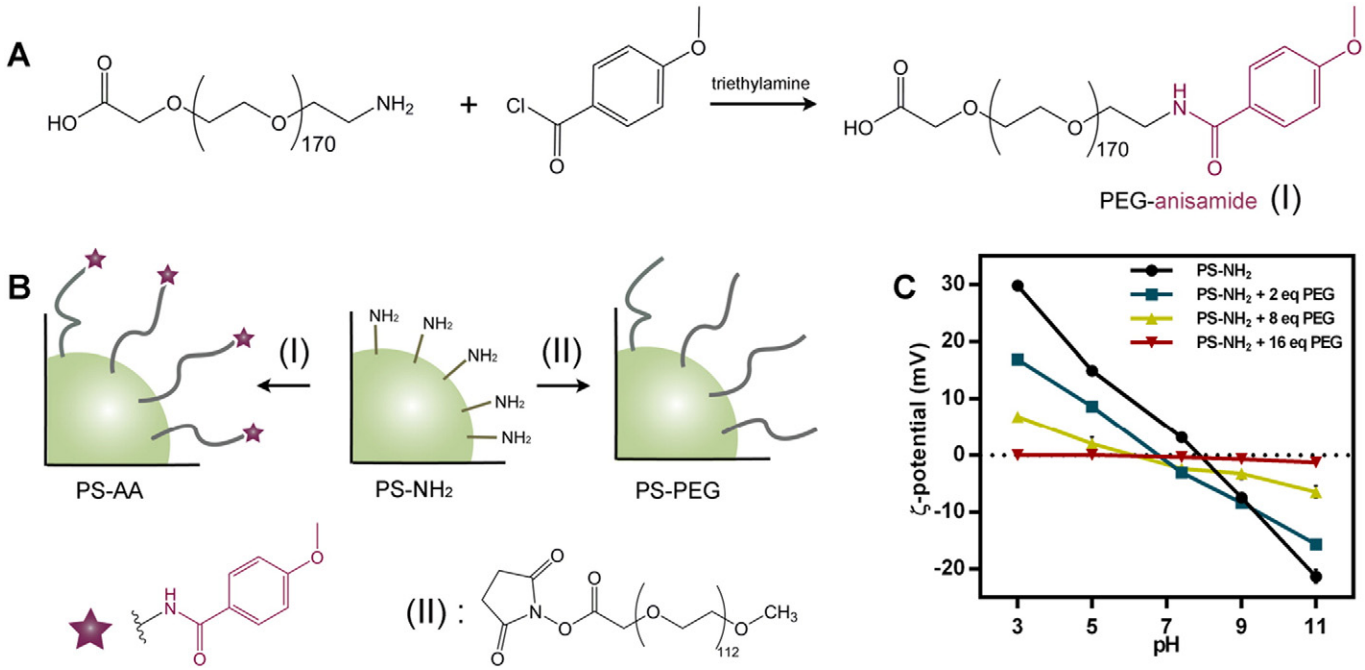

Fig. 1. Particle design and characterization. (A) Synthesis of anisamide-PEG-carboxylate. (B) Preparation of functionalized particles, PEGylated (PS-PEG) or PEGylated and anisamide-targeted (PS-AA). (C) Monitoring of particle PEGylation by ζ-potential measurement after reacting PS-NH_2 with various amounts of PEG-NHS. Results are expressed as mean ± S.D. (n = 3).

containing anisamide in their chemical structure have been shown to deposit in higher amounts in tumors following i.v. injection in rodents and have thus been proposed as tumor-imaging agents [12,13]. It has been hypothesized that the increased tumor deposition was a consequence of those molecules' affinity for a receptor reported to be highly expressed by tumor cells, the Sigma-1 receptor (σ_1R) [14–16]. Following the initial publication reporting the grafting of anisamide onto the surface of liposomes and subsequent enhanced uptake by tumor cells *in vitro* as well as increased deposition in the tumor *in vivo* [11], the ligand has been utilized to decorate many different types of particles. For example, polyester nanoparticles [17], cyclodextrin nanoparticles [18], lipid-coated calcium phosphate nanoparticles [19] and silica nanoparticles [20] have been employed and this strategy has been shown to enhance uptake by various tumor cell lines *in vitro* as well as in tumor tissues *in vivo* [18,21–26]. It should be noted that the anisamide initially suggested by Huang and colleagues in 2004 was the [2-(4′-methoxybenzamido)]ethylamine, which was attached on PEG [11]. However, in several publications, including those from other groups but also two recent from Huang and coworkers, the 4-methoxybenzamide moiety without the ethylamine part was coupled on PEG and similar enhancement of cell uptake of the delivery systems was reported [17,18,20,27–29]. The results obtained with this ligand, also named anisamide, imply that the ethylamine part is not necessary for the enhancement of cell uptake of the decorated particles.

In all previous reports, the presumed cell component interacting with anisamide is the σ_1R, based on the binding of the iodobenzamides used in tumor imaging studies. However, to date no thorough characterization of the interaction between the receptor and the molecule has been performed. The goal of this work was to examine whether σ_1R plays a role in the internalization of the anisamide-tethered particles. Towards this aim, we designed PEGylated fluorescent poly(styrene) particles and coated them with 4-methoxybenzamide. We then investigated how the ligand influences the cellular uptake of the particles and whether σ_1R is implicated in this process.

2. Materials and methods

2.1. Chemicals and reagents

Heterobifunctional amine-PEG-carboxylate (M_n = 7500 Da, PDI = 1.02) and monofunctional methoxy-PEG-succinimidyl carboxymethyl ester (methoxy-PEG-NHS) (M_n = 5000 Da, PDI = 1.03) were purchased from JenKem Technology (Beijing, China). (+)-SKF-10,047 hydrochloride (purity >98%) was obtained from TOCRIS Bioscience (Bristol, UK). B16-F10, RAW 264.7 and 4T1 cell lines were purchased from ATCC (Manassas, VA). FluoSpheres® amine-modified microspheres (1 μm, yellow green fluorescent), Dulbecco's Modified Eagle Medium (DMEM) with GlutaMAX® (high glucose), penicillin/streptomycin solution (10,000 units/mL penicillin and 10,000 μg/mL streptomycin), fetal bovine serum (FBS), phosphate buffered saline pH 7.4 (PBS) (composition in mM: 155 NaCl, 1.05 KH_2PO_4 and 2.97 Na_2HPO_4–$7H_2O$), trypsin/EDTA 0.05% and 0.25%, Lipofectamine® 2000 and siRNA targeting σ_1R (Silencer® Select, siRNA ID: s71116, Ambion®) were all purchased from Life Technologies (Carlsbad, CA). Osmium tetroxide and LR White® were purchased from Polysciences Inc. (Eppelheim, Germany). All other chemicals were purchased from Sigma-Aldrich (St. Louis, MO) and used as received.

2.2. Synthesis of anisamide-PEG-carboxylate

Amine-PEG-carboxylate (200 mg, 0.027 mmol) was dissolved in 10 mL dichloromethane. 4-methoxybenzoyl chloride (50 μL, 0.37 mmol) and triethylamine (50 μL, 0.36 mmol) were added to the solution and the mixture was stirred for 24 h at room temperature (RT) under inert argon atmosphere. The solvent was removed by rotary evaporation and the polymer was purified by Gel Permeation Chromatography using a PD MidiTrap® G-25 column (GE Healthcare, Buckinghamshire, UK).

2.3. Preparation of PEGylated anisamide-targeted (PS-AA) and PEGylated control (PS-PEG) poly(styrene) particles

Yellow-green fluorescent poly(styrene) amine-modified particles of 1-μm diameter (PS-NH_2) (2 mg) were washed twice with water by centrifugation and then dispersed in 1 mL of DMSO and sonicated for 10 min in a bath sonicator. Various amounts of methoxy-PEG-NHS were added and left to react for 24 h under stirring at RT. After reaction, the mixture was diluted in 5 mL of water and centrifuged (5000 × *g*, 15 min, 15 °C) to remove the DMSO. The particles were collected at the bottom and resuspended in water. The washing step was repeated 4 times to remove the excess of unreacted polymer. Finally, the particles were resuspended in 1 mL of PBS pH 7.4, resulting in a final concentration of 2 mg/mL. Anisamide-targeted particles were prepared by reaction of PS-NH_2 (2 mg) with anisamide-PEG-carboxylate (1.5 mg), together with a coupling reagent, HATU (1-[Bis(dimethylamino)methylene]-1H-1,2,3-triazolo[4,5-b]pyridinium 3-oxid hexafluorophosphate) (0.15 mg) and triethylamine (0.7 mg) to activate the carboxylic groups. After stirring of the mixture for 24 h at RT, the particles were washed for DMSO removal and resuspended in PBS as described above to a final concentration of 2 mg/mL. Particle suspensions were sonicated in a Sonorex Super RK 31 H ultrasonic bath (35 kHz, 70 W, Bandelin Electronics, Berlin, Germany) for 15 min before use.

2.4. Particle characterization

Particle size and ζ-potential were determined by dynamic light scattering (DLS) and laser Doppler anemometry respectively, using a DelsaNano C Particle Analyzer (Beckman Coulter, Krefeld, Germany). The CONTIN method was used to calculate the hydrodynamic diameter of the particles. ζ-potential was measured at different pH values by diluting the particles in the corresponding buffer at a particle concentration of 50 μg/mL.

2.5. Cell culture

B16-F10 (murine melanoma), RAW 264.7 (murine macrophage-like) and 4T1 (murine mammary carcinoma) cells were grown in DMEM with GlutaMAX® (high glucose) supplemented with 10% (*v*/*v*) FBS, 100 units/mL penicillin and 100 μg/mL streptomycin. Cells were kept at 37 °C in a humidified atmosphere containing 5% CO_2.

2.6. In vitro particle uptake

Cells were seeded in 12-well plates at a density of 150,000 cells per well for B16-F10 and 4T1 cells and 400,000 cells per well for RAW 264.7 cells. Twenty-four hours later, the particles (10 μL, 20 μg) were added to the medium (final volume 1 mL per well) and incubated for 4 h. The cells were then washed 4 times with PBS to remove non-internalized particles and were prepared for flow cytometry as follows. Briefly, B16-F10 and 4T1 cells were detached with 0.05% Trypsin/EDTA for 5 min at 37 °C, while RAW 264.7 cells were gently scraped from the plate surface. Detached cells were collected in complete medium and kept on ice for all subsequent steps. The samples were centrifuged (300 × *g*, 4 °C, 10 min), the supernatant was discarded and the cells were washed twice with ice-cold PBS supplemented with 0.5% *w*/*v* bovine serum albumin (BSA) and 2 mM EDTA. The cells were then resuspended in ice-cold PBS supplemented with 0.5% *w*/*v* BSA and 2 mM EDTA for the flow cytometry analysis. The fluorescence measurement was performed in a FACSCanto® Flow Cytometer (BD Biosciences, San Jose, CA) and a minimum of 10,000 events per sample was recorded using FACSDiva® Software (BD Biosciences). A 488-nm laser was used for excitation and the FITC channel (530/30 nm) was used for the detection of the fluorescence emission. The percentage of fluorescence-positive cells was analyzed using the FlowJo software (Tree Star Inc., Ashland, OR).

For σ_1R-ligand competition studies, 30 μM haloperidol or 100 μM (+)-SKF-10,047 were added to the cells together with the particles and incubated for 4 h. The cell uptake was assessed by flow cytometry as described above.

2.7. Live cell confocal microscopy

B16-F10 cells expressing TdTomato fluorescent protein [30] were plated onto 2-well Lab-Tek® II Chamber Slides (Nunc, Rochester, NY) at a density of 150,000 cells per well (final volume 1 mL per well) and left to grow at 37 °C, 5% CO_2 for 24 h. PS-AA particles (10 μL, 20 μg) were added to the cells for 2, 4 and 24 h. Cells were washed twice with PBS and imaged in DMEM without Phenol Red (Life Technologies) using a Zeiss Axio Observer Z1 inverted spinning disk confocal microscope (Carl Zeiss, Oberkochen, Germany) equipped with a Zeiss C-Apochromat M27 63×/1.2NA water objective. Excitation lasers 488 nm and 561 nm were used for particle and TdTomato fluorescence respectively with emission filters 520/35 and 617/73, respectively. A z-stack of 25 slices with slice spacing of 0.3 μm was acquired using the ZEN 2012 Blue (Zeiss) software and processed with ZEN 2012 Blue and Image J software (National Institutes of Health, Bethesda, MD).

2.8. Transmission electron microscopy (TEM)

B16-F10 cells were seeded in 12-well plates at a density of 150,000 cells per well (final volume 1 mL) and were treated the next day with PS-AA (20 μL, 40 μg) for 12 h. Cells were washed with PBS 4 times and then trypsinized, spun down to form a pellet and fixed with 2.5% glutaraldehyde in PBS for 2 h. The cell pellet was washed in PBS, and post-fixed in 1% osmium tetroxide in PBS for 30 min, then washed twice in PBS, followed by 90 min in 1% aqueous uranyl acetate. Subsequently, the cells were dehydrated through a graded series of ethanol (30 min each in 30%, 70% and 100% ethanol), before infiltration with LR White®: 1 h in 30% LR White® in ethanol, overnight in 70% LR White® in ethanol and twice 4 h in 100% fresh LR White®. The samples were polymerized at 60 °C for 72 h. After polymerization, 60 nm sections were cut using an ultramicrotome (Leica Microsystems, Wetzlar, Germany) and post-stained with uranyl acetate (2% aqueous solution) and Reynold's lead citrate. Transmission electron microscopy was performed at 100 kV (FEI Morgagni268, FEI Company, Hillsboro, OR).

2.9. Co-administration of particles and B16-F10 cells in vivo

In vivo experiments were performed in accordance with the animal protocol approved by the Kantonales Veterinaeramt Zurich (protocol: 11/2012). B16-F10 cells expressing TdTomato fluorescent protein [30] (500,000 cells) were mixed with PS-AA or PS-PEG particles (1 μL, 2 μg) in a final volume 50 μL of PBS, incubated in humidified atmosphere at 37 °C, 5% CO_2 for 15 min and subsequently injected intradermally in the hind flank of 8-week-old female C57BL/6J albino mice (Jackson Laboratories, Bar Harbor, ME). Fourteen days after inoculation, the tumors were excised and passed through a sterile 40-μM BD Falcon® nylon cell strainer (BD Biosciences) and re-suspended in ice-cold PBS supplemented with 0.5% *w*/*v* BSA and 2 mM EDTA for flow cytometry analysis. The fluorescence measurement was performed using an LSRFortessa® Flow Cytometer (BD Biosciences) and a minimum of 30,000 events per sample was recorded using FACSDiva® Software (BD Biosciences). A 488-nm laser was used for excitation and the FITC channel (530/30 nm) was used for the detection of the fluorescence emission of the particles, while a 561-nm laser for excitation and the PE channel (586/15 nm) for the fluorescence emission was used for TdTomato. The percentage of double-positive cells for particle fluorescence and TdTomato was quantified using the FlowJo software (Tree Star Inc.).

2.10. σ_1R knock-down and particle uptake

B16-F10 cells were seeded in 12-well plates at a density of 40,000 cells per well. After 24 h, the cells were transfected with 0.25 μg (18.5 pmol) of Ambion Silencer® Select σ_1R siRNA (sequence: sense 5′-ACU UCG UCU UCU CUA GAG Att-3′ and antisense 5′-UCU CUA GAG AAG ACG AAG Utt-3′) using Lipofectamine® 2000 Reagent (Life Technologies). In detail, the siRNA was mixed with Lipofectamine® in serum-free antibiotics-free medium at a ratio of siRNA to Lipofectamine® 1: 3 (*w*/*w*) for 20 min at RT, then diluted in serum-containing antibiotics-free medium (0.5 mL final volume) and added to the cells. Twenty-four hours later, the medium was replaced with fresh complete medium (with FBS and antibiotics) and the cells were grown for 48 h before proceeding to the particle uptake experiment as described in the "*In vitro* particle uptake" section or to cell lysis for subsequent Western blot analysis of σ_1R expression levels.

2.11. Effect of σ_1R ligands on cell growth and adhesion — real-time cell analysis

The effect of the σ_1R ligands haloperidol and (+)-SKF-10,047 on B16-F10 cells was studied using a label-free real-time impedance-based cell analysis system, the xCELLigence RTCA DP Instrument (ACEA Biosciences Inc., San Diego, CA), which was placed in a humidified cell incubator at 37 °C and 5% CO_2. This instrument monitors the cell number, morphology, and adhesion degree on the plate surface by measuring the relative change in electrical microimpedance on the well surface of the plates and expresses it as a unitless parameter, the Cell Index (CI) value [31]. B16-F10 cells were seeded in E-Plate-VIEW 16-well plates (Roche Diagnostics, Mannheim, Germany) in culture medium at a density of 10,000 cells per well. Background impedance was measured in 100 μL culture medium per well. Approximately 20 h after cell seeding, the medium was replaced by fresh medium containing various concentrations of haloperidol or (+)-SKF-10,047. Stock solutions of haloperidol in DMSO were prepared so that the solvent percentage was kept at 0.1% for all tested concentrations on the cells. (+)-SKF-10,047 stock solutions were prepared in water. The CI was monitored and recorded every 15 min over 24 h with the RTCA DP analyzer and the RTCA Software (ACEA Biosciences Inc.). The CI values were normalized at the time-point of addition of each compound and the normalized CI was used for graphical representation of the results. For haloperidol-treated cells, the normalized CI values were used to plot the dose–response curves at 4 and 24 h following addition of the drug. EC_{50} values (concentration of haloperidol resulting in 50% reduction of the CI value relative to solvent control CI value) were calculated after data fitting using GraphPad Prism version 6.01 (GraphPad Software, La Jolla, CA).

2.12. σ_1R Western blot

Seventy-two hours after σ_1R siRNA transfection, B16-F10 cells were washed with PBS and cell lysates were prepared in lysis buffer (20 mM Tris–HCl pH 7.7, 150 mM NaCl, 5 mM EDTA, 1% *v*/*v* Triton X-100, 25 mM NaF, 1 mM phenylmethylsulfonyl fluoride, 1 mM sodium orthovanadate) supplemented with Complete® EDTA-free protease inhibitors' cocktail (Roche Diagnostics, Mannheim, Germany) on ice for 15 min. Cell debris were removed by centrifugation at 15,000 × *g* for 15 min at 4 °C and protein concentration in the supernatants was determined using the microBCA assay (ThermoFischer Scientific, Waltham, MA). Thirty micrograms of total protein per sample were resolved by 12% SDS-PAGE and transferred to an Immun-Blot® PVDF membrane (Bio-Rad, Hercules, CA). The membrane was blocked with Tris-buffered saline containing 0.1% (*v*/*v*) polysorbate-20 and 5% skim milk (blocking buffer) for 1 h at RT. The membrane was cut in two at 35 kDa, determined by molecular weight marker. The lower part containing σ_1R (25 kDa) was incubated overnight at 4 °C with mouse σ_1R monoclonal antibody B-5 (Santa Cruz Biotechnology, Dallas, TX) diluted 1:1000 in blocking buffer. The upper part containing β-actin (loading control) was incubated with rabbit polyclonal anti-β-actin antibody (Abcam, Cambridge, UK) at a dilution of 1:4000 in blocking buffer. Membranes were washed 3 times for 5 min with Tris-buffered saline containing 0.1% (*v*/*v*) polysorbate-20 and then incubated with the secondary antibodies: horseradish peroxidase-conjugated polyclonal goat anti-mouse IgG (Dako, Glostrup, Denmark) for σ_1R and horseradish peroxidase-conjugated polyclonal goat anti-rabbit IgG for β-actin (Abcam), for 1 h in blocking buffer. Membranes were washed 3 times for 5 min with Tris-buffered saline containing 0.1% (*v*/*v*) polysorbate-20 and protein bands were detected with ImmunoCruz® Western blotting Luminol Reagent (SantaCruz Biotechnology) and revealed on Super RX X-Ray films (Fujifilm, Tokyo, Japan), using an AGFA Curix 60 film processor (AGFA, Mortsel, Belgium). Semi-quantification of the σ_1R band intensities was performed using Image J software.

2.13. σ_1R immunostaining

σ_1R of B16-F10 cells was immunostained and the staining was assessed by flow cytometry and by fluorescence microscopy. For flow cytometry analysis of σ_1R staining, B16-F10 cells were seeded in 12-well plates at a density of 200,000 cells per well. The next day the cells were washed once with PBS, detached with Cell Dissociation Buffer, enzyme-free PBS (Life Technologies) for 10 min, collected in culture medium and centrifuged (300 × *g*, 4 °C, 10 min) to remove the supernatant. Samples were kept on ice during the entire procedure. σ_1R immunostaining was performed on living and on fixed/permeabilized cells. For staining on living cells, σ_1R antibody (Santa Cruz Biotechnology) or mouse $IgG_{1\kappa}$ isotype control antibody (Sigma-Aldrich) was added at a final concentration of 1 μg/mL in ice-cold PBS supplemented with 0.5% *w*/*v* BSA and 2 mM EDTA for 1 h. Cells were washed twice by centrifuging and then incubated with secondary Alexa Fluor® 488-conjugated goat anti-mouse IgG antibody (Life Technologies) (1 μg/mL in PBS 0.5% *w*/*v* BSA) for 45 min. After washing 3 times with PBS containing 0.5% *w*/*v* BSA and 2 mM EDTA, the cells were resuspended in the same buffer for the subsequent flow cytometry analysis. For σ_1R staining on fixed and permeabilized cells, 100% ice-cold methanol was used as fixation/permeabilization reagent after cell detachment from the plates for 10 min. The cells were washed with PBS and incubated for 1 h with blocking buffer (PBS containing 0.05% (*v*/*v*) polysorbate-20 and 5% (*v*/*v*) goat serum), to reduce non-specific staining. Primary antibodies (σ_1R antibody or $IgG_{1\kappa}$ isotype control) were diluted in blocking buffer at a final concentration of 1 μg/mL and added on the cells for 1 h. Cells were washed twice with PBS containing 0.05% polysorbate-20 and incubated with the secondary Alexa Fluor® 488-conjugated goat anti-mouse IgG antibody (Life Technologies) at 1 μg/mL in blocking buffer for 45 min. The cells were washed twice with PBS containing 0.05% polysorbate-20 and then resuspended in PBS supplemented with 0.5% *w*/*v* BSA and 2 mM EDTA. The flow cytometry measurement was performed using a FACSCanto® Flow Cytometer (BD Biosciences) and a minimum of 10,000 events per sample was recorded using FACSDiva® Software (BD Biosciences). A 488-nm laser was used for excitation and the FITC channel (530/30 nm) was used for the detection of the fluorescence emission. A minimum 10,000 events per sample was recorded and the fold-change of the mean fluorescence intensity (MFI) compared to the unstained samples was calculated using the FlowJo software (Tree Star Inc.).

For microscopic observation of σ_1R-immunostaining, B16-F10 cells were seeded on round glass coverslips of 18-mm diameter in 12-well plates at a density of 60,000 cells per well. The next day, the cells were washed once with PBS and fixed/permeabilized with 100% ice-cold methanol for 10 min. After two washes with PBS, the cells were kept in blocking buffer (PBS containing 0.05% (*v*/*v*) polysorbate-20 and 5% (*v*/*v*) goat serum) for 1 h to block non-specific binding of the antibodies. Cells were incubated with σ_1R antibody (Santa Cruz

Biotechnology) or $IgG_{1\kappa}$ isotype control antibody (Sigma-Aldrich) at a final concentration of 2 μg/mL in blocking buffer for 2 h at RT. Samples were washed 3 times with PBS containing 0.05% polysorbate-20 and then incubated with the secondary Alexa Fluor® 488-conjugated goat anti-mouse IgG antibody (Life Technologies) at 2 μg/mL in blocking buffer for 45 min at RT. After washing the cells 3 times with PBS containing 0.05% polysorbate-20, the cell nuclei were stained with Hoechst solution 2 μg/mL in PBS for 5 min. The cells were washed twice with PBS and twice with water and the coverslips were mounted on glass slides with Mowiol® 4–88 mounting medium (Merck Millipore, Billerica, MA). Image acquisition was performed using a Leica DMI 6000 B inverted epifluorescence microscope (Leica Microsystems) equipped with a Leica DFC365 FX digital camera (Leica Microsystems). A Leica 40×/0.75 HCX PL FLUOTAR objective with appropriate sets (Hoechst: filter set A4: ex. BP 360/40 em. BP 470/40, σ_1R: filter set L5: ex. BP 480/40 em. BP 527/30) was used. Images were processed with LAS AF software (Leica) and Image J software.

2.14. Statistical analysis

All statistical analyses were performed using the GraphPad Prism software. When the number of replicates was lower than five, Gaussian distribution was assumed and the results were analyzed using ANOVA followed by the appropriate multiple comparisons test. For the *in vivo* experiment, the non-parametric Mann–Whitney test was used. The level of statistical significance for all experiments was fixed at $p \leq 0.05$.

3. Results

3.1. Particle functionalization

In this study, commercially-available poly(styrene) particles of 1-μm diameter, labeled with a proprietary yellow-green fluorescent dye (Ex/Em: 505/515) and bearing primary amine groups on the surface ($PS\text{-}NH_2$) were used as the starting material. The fluorescent dye was essential for the detection of the particles in subsequent experiments, while the reactive amine groups present on the surface were utilized for the particle functionalization. The surface was modified with an anisamide-PEG-carboxylate conjugate, synthesized as shown in Fig. 1A and characterized by ^{1}H NMR (Supplementary Fig. S1) and FTIR (Supplementary Fig. S2) spectroscopies, and thus PEGylated and targeted particles (PS-AA) (Fig. 1B) were obtained. PEGylated control particles without anisamide (PS-PEG) (Fig. 1B) were prepared by reacting $PS\text{-}NH_2$ with methoxy-PEG-NHS in DMSO. The PEGylation reaction was monitored by adding various amounts of methoxy-PEG-NHS and measuring the ζ-potential at different pH values (Fig. 1C). $PS\text{-}NH_2$ particles presented a highly positive ζ-potential value (+30 mV) at pH 3, which decreased with the increase of pH, reaching a value of +5 mV at pH 7 and −21 mV at pH 11. After reaction with excess amounts of PEG-NHS, the ζ-potential ranged from 0 mV at pH 3 to −1 mV at pH 11 (Fig. 1C), indicating the good shielding effect of PEG chains over the residual positive charges on the particle surface. The measurement of ζ-potential at pH 3 was therefore chosen to monitor the efficacy of the chemical modifications over $PS\text{-}NH_2$. Similarly, the PS-AA exhibited a ζ-potential value of −1 mV at pH 3, which indicated adequate PEGylation.

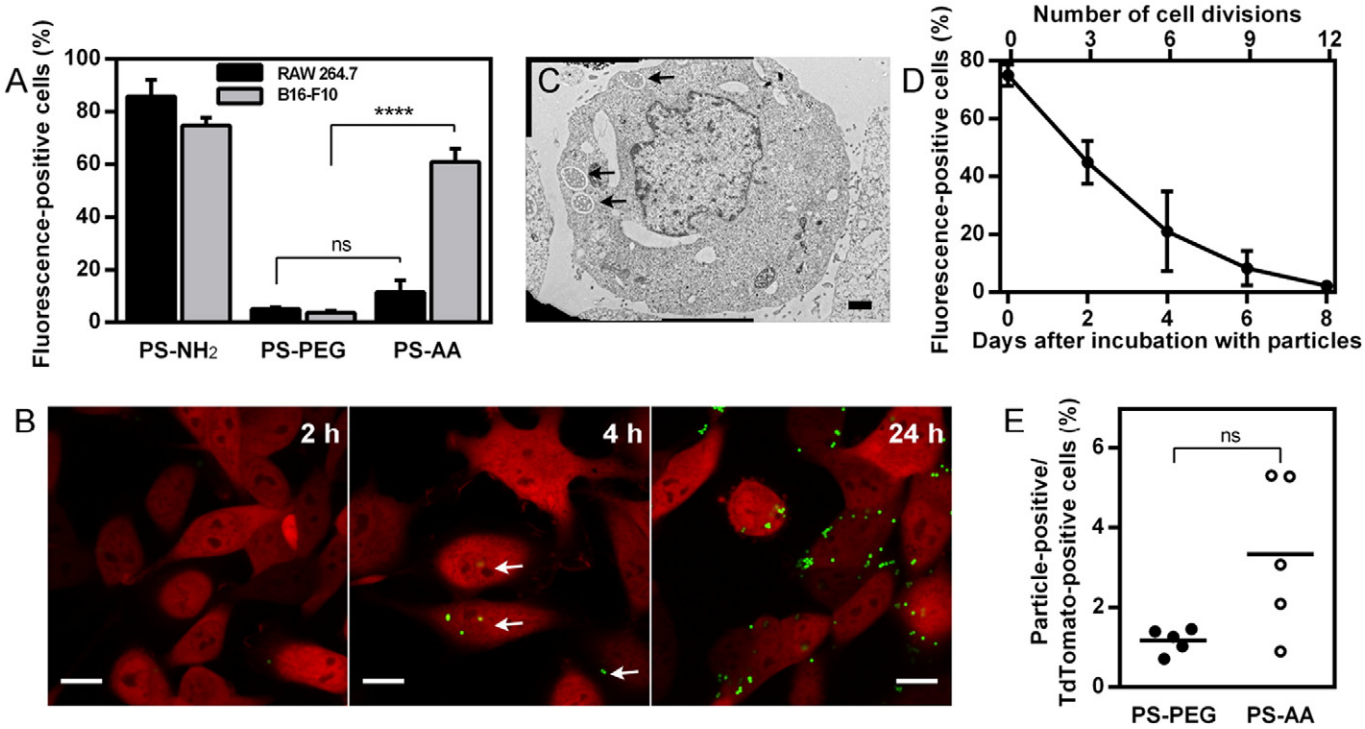

Fig. 2. Cellular uptake of modified and non-modified particles. (A) Flow cytometry results of *in vitro* uptake by B16-F10 and RAW 264.7 cells. Results are expressed as mean ± S.D. n = 3, (****) $p < 0.0001$ and (ns) $p > 0.5$ *vs.* indicated bar. (B) Confocal microscopy pictures showing time-dependent uptake of PS-AA. Middle slices of the acquired z-stack are presented. Red: TdTomato-expressing B16-F10 cells, green: particles. Scale bar: 15 μm. White arrows indicate the endocytosed particles. (C) TEM image of a B16-F10 cell with internalized particles. Scale bar: 1 μm. Black arrows indicate the presence of PS-AA in the cell. (D) Assessment of particle-positive cells after several divisions of cells having internalized PS-AA particles, as determined by flow cytometry. Results are expressed as mean ± S.D. (n = 4). (E) Uptake of PS-PEG and PS-AA by B16-F10 in *in vivo* conditions, after co-injection of particles and cells in the hind flank of female C57BL/6J albino mice. The tumors were excised 14 days after tumor inoculation and the particle-positive tumor cells were quantified by flow cytometry. n = 5, (ns) $p < 0.5$.

3.2. In vitro particle uptake

The cellular uptake of the functionalized and non-functionalized particles was evaluated using B16-F10 murine melanoma cells as a model cancer cell line, which have been shown in preceding publications to take up anisamide-decorated nanoparticles [32,33]. A non-cancerous cell line, the murine macrophage-like RAW 264.7, was used as a control. Cells were incubated with the different types of particles for 4 h in the presence of serum. As seen in Fig. 2A, the non-PEGylated PS-NH_2 particles were highly taken up by both cell lines. After 4 h of incubation, 82% of RAW 264.7 cells and 75% B16-F10 cells had taken up PS-NH_2 particles, probably due to non-specific interactions with the cells. Particle PEGylation drastically decreased the uptake by the melanoma cells (down to 5% of particle-positive cells), as well as by the macrophages (3% of particle-positive cells), due to the shielding effect of PEG. Grafting of the anisamide moiety at the distal end of the PEG chain resulted in enhancement of uptake by the B16-F10 cells (65% of particle-positive cells), but did not significantly affect the uptake by the macrophages (Fig. 2A). The observed preferential uptake by the B16-F10 cells compared to the non-cancerous RAW 264.7 cells suggested a selective interaction of the targeting ligand with some tumor cells, as previously reported [11,32,34,35]. It should be noted that the PEG chain length between PS-PEG and PS-AA particles is different because of the availability of the commercially-found functionalized PEGs needed for this work. It was verified that the different length of PEG did not influence the uptake (Supplementary Fig. S3).

Internalization of PS-AA particles by B16-F10 cells after 4 h of incubation was confirmed by confocal microscopy (Fig. 2B and Supplementary Fig. S4), as well as by the Trypan Blue fluorescence quenching method incorporated in the flow cytometry measurement (Supplementary methods and Supplementary Fig. S5). The presence of PS-AA particles intracellularly was also shown by TEM (Fig. 2C). After internalization, the particles remained inside the cells after several cell divisions and could be traced up to 6 days, as revealed by flow cytometry and fluorescence microscopy (Supplementary methods, Fig. 2D and Supplementary Fig. S6).

Finally, the particle uptake experiment was performed in *in vivo* conditions, by co-injecting tumor cells and PS-PEG or PS-AA particles intradermally in mice for tumor inoculation. The aim was to assess the uptake under conditions favorable for the interactions between tumor cells and particles. Tumors were excised and the cells containing particles were quantified. The results revealed a trend towards increased cellular uptake of PS-AA particles compared to PS-PEG, although statistical significance was not achieved (Fig. 2E).

3.3. Involvement of the σ_1R

To investigate whether the tumor-targeting properties of the anisamide-tethered particles are associated with the σ_1R, we sought to examine the interaction of anisamide with this receptor. We initially attempted to reproduce an experiment that had been performed in preceding studies to demonstrate the involvement of the σ_1R in the internalization of the anisamide-decorated nanocarriers. In previous reports, the anisamide-functionalized particles were incubated with the cells either in the presence of a σ_1R antagonist, haloperidol [24,28,32,34], or after pre-incubation of the cells with this compound [11,18,19]. Displacement of the particles by haloperidol on the cell binding sites would suggest a competitive binding for the σ_1R. Here, the same experiment was also conducted using a σ_1R agonist, (+)-SKF-10,047 [36]. We first examined the toxicity of these two σ_1R ligands on the B16-F10 cells using a real-time cell analysis system, the xCELLigence [31]. The cells were incubated with various concentrations of the compounds and the CI was monitored over 24 h. The CI is a parameter that depends on the cell number, morphology and adhesion degree, with higher number of cells and higher spreading of the cells on the plate surface leading to higher CI values [31]. As shown in Fig. 3A, increasing concentrations of

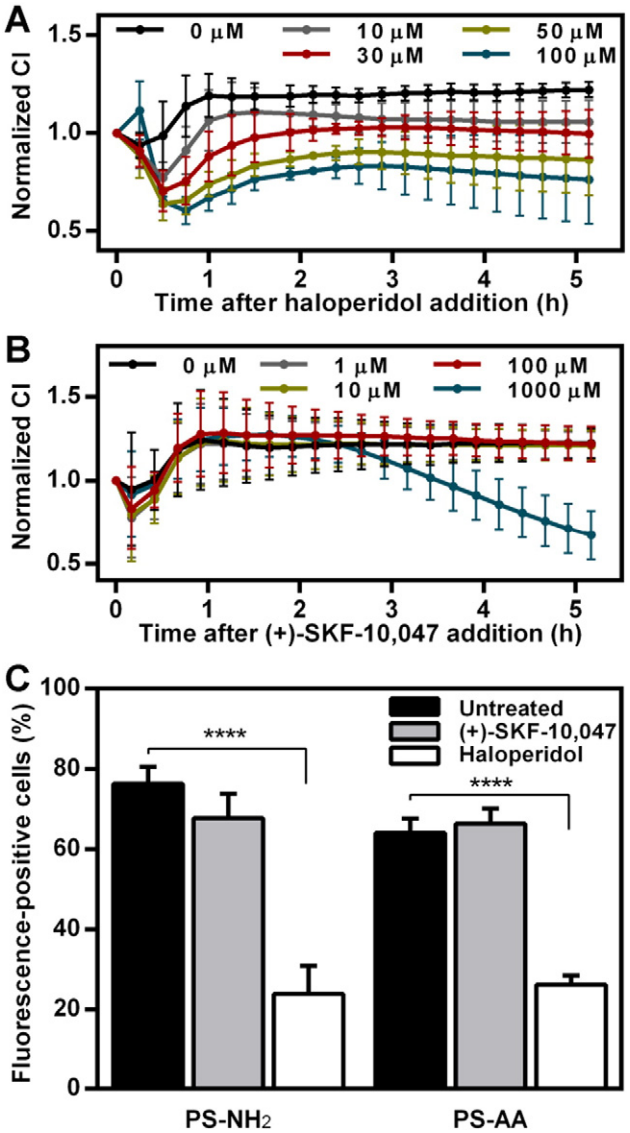

Fig. 3. Particle uptake competition with σ_1R ligands. Toxicity of (A) haloperidol and (B) (+)-SKF-10,047 respectively on the B16-F10 cells using the xCELLigence system. The CI was normalized for t = 0 (time-point of addition of the drug). Results are expressed as mean ± S.D. (n = 4). (C) Effect of the σ_1R ligands on the uptake of PS-NH_2 and PS-AA particles. Results are expressed as mean ± S.D. (n = 3). (****) $p < 0.0001$ *vs.* indicated bar.

haloperidol led to decreased values of the CI compared to untreated cells, indicating a cytotoxic effect of the compound in the μM range, an effect which was not observed with the presence of (+)-SKF-10,047 (Fig. 3B). A haloperidol concentration of 50 μM, which has been used in the uptake competition experiment in most of the previous reports [24,28,32,34], had an important effect on cell growth and adhesion after 4 h. A concentration of 30 μM, which had a small effect on the CI value (Fig. 3A), was therefore used here for the particle uptake competition experiment. This concentration was also the lowest concentration used in previous studies [11]. As presented in Fig. 3C, while the presence of (+)-SKF-10,047 did not affect the endocytosis of any type of particle tested, haloperidol led to a reduction of uptake not only of PS-AA but also of PS-NH_2 particles. The next step was to evaluate the effect of haloperidol on three σ_1R-independent endocytosis markers: dextran, human transferrin and lactosylceramide, which are internalized by the process of macropinocytosis [37], clathrin-dependent and clathrin-independent endocytosis, respectively [38]. Haloperidol led to a

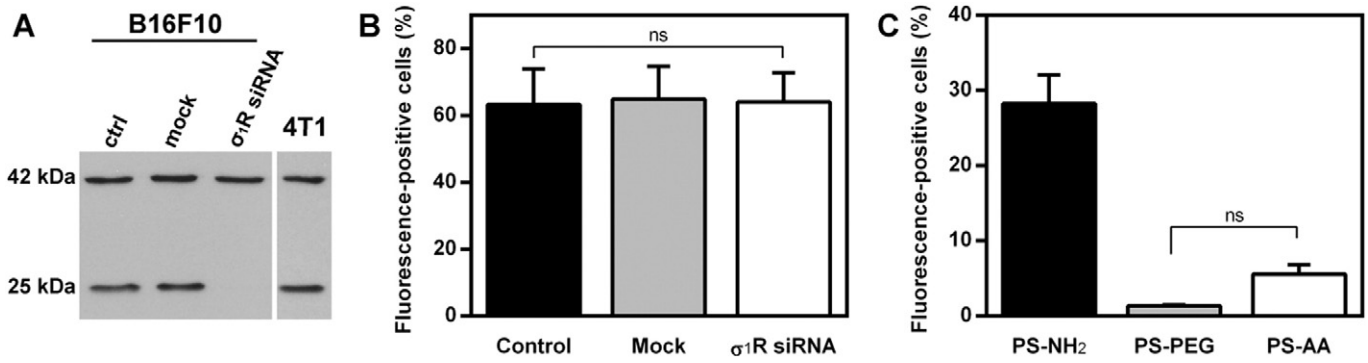

Fig. 4. σ_1R expression and particle uptake. (A) Western blot of σ_1R expression in B16-F10 and 4T1 cells. B16-F10 cells were treated with σ_1R siRNA and the protein levels were assessed 72 h post-transfection. Mock transfected cells were treated with Lipofectamine® but no siRNA. σ_1R: 25 kDa, β-actin: 42 kDa. (B) Anisamide-targeted particle uptake by σ_1R siRNA-treated and non-treated B16-F10 cells. Results are expressed as mean ± S.D. n = 3, (ns) $p > 0.05$. (C) Particle uptake by 4T1 cells. Results are expressed as mean ± S.D. (n = 3). (ns) $p > 0.05$ *vs.* indicated bar.

significant reduction of internalization of dextran and transferrin (Supplementary methods and Supplementary Fig. S7), suggesting a non-specific endocytic inhibition effect of haloperidol.

Since the competition studies with haloperidol and (+)-SKF-10,047 did not reveal any specificity of anisamide for σ_1R, we investigated the correlation between the σ_1R expression levels and the extent of targeted particle uptake, with the aim of further elucidating the interaction of the anisamide-decorated particles with the cells. We used a siRNA approach to down-regulate the expression of σ_1R and then performed the particle uptake experiment. Seventy-two hours after σ_1R siRNA treatment, the residual expression of the receptor on protein level was less than 10%, as revealed by Western blot (Fig. 4A). However, uptake by B16-F10 cells with down-regulated σ_1R was the same as the uptake observed by cells not treated with σ_1R siRNA (Fig. 4B). In addition, another murine cell line, the 4T1 mammary carcinoma cell line, which expresses the receptor in similar levels as the B16-F10 (Fig. 4A), did not present increased uptake of the anisamide-decorated particles (Fig. 4C). It is worth noting that the internalization of the PS-NH_2 particles was also lower compared to the B16-F10 cells (Fig. 4C).

Finally, we performed immunostaining of the σ_1R on B16-F10 cells for flow cytometry analysis and for fluorescence microscopy in order to investigate its localization in these cells. As shown by the flow cytometry results (Fig. 5A and Supplementary Fig. S8A), immunostaining of the receptor on intact, live cells did not show any fluorescence signal, while a cell surface receptor (transferrin receptor, expressed by B16-F10 cells [39]) was successfully stained in the same experimental conditions (Supplementary methods and Supplementary Fig. S8B). However, after fixation/permeabilization using methanol, the fluorescence signal given by σ_1R antibody was very pronounced compared to the IgG isotype control antibody (Fig. 5A and Supplementary Fig. S8A). Moreover, microscopic observation of fixed and permeabilized cells after σ_1R-immunostaining revealed the intracellular presence of the receptor, mostly in the perinuclear space of the B16-F10 cells (Fig. 5B, C), while an isotype control antibody did not give any fluorescence signal (Fig. 5D). No fluorescence signal was observed on the plasma membrane. In addition, after cell fixation with paraformaldehyde, which fixes but does not permeabilize the cells, no staining of σ_1R on the cell surface was apparent (Supplementary methods and Supplementary Fig. S9).

4. Discussion

In this work, poly(styrene) fluorescent particles of 1-μm diameter were used as a tool to study the interaction of anisamide with melanoma cells. Liposomes of size 200 nm were initially tested (Supplementary methods and Supplementary Figs. S10 and S11), for comparison purposes in order to include an anisamide-decorated system that was closer in terms of size to what had been previously reported in the literature [11,17,18,22,23]. The anisamide-decorated liposomes presented significantly higher uptake compared to PEGylated non-targeted ones. However, this difference in uptake was relatively small, not significant in the presence of FBS and therefore insufficient to adequately identify the role of σ_1R in the uptake process. For this reason, the main body of work was performed with the 1-μm poly(styrene) particles which exhibited a very high uptake compared to the non-targeted particles.

Poly(styrene) PEGylated particles decorated with anisamide were shown to be efficiently internalized *in vitro* by B16-F10 melanoma cells but not by macrophages. These results are in agreement with

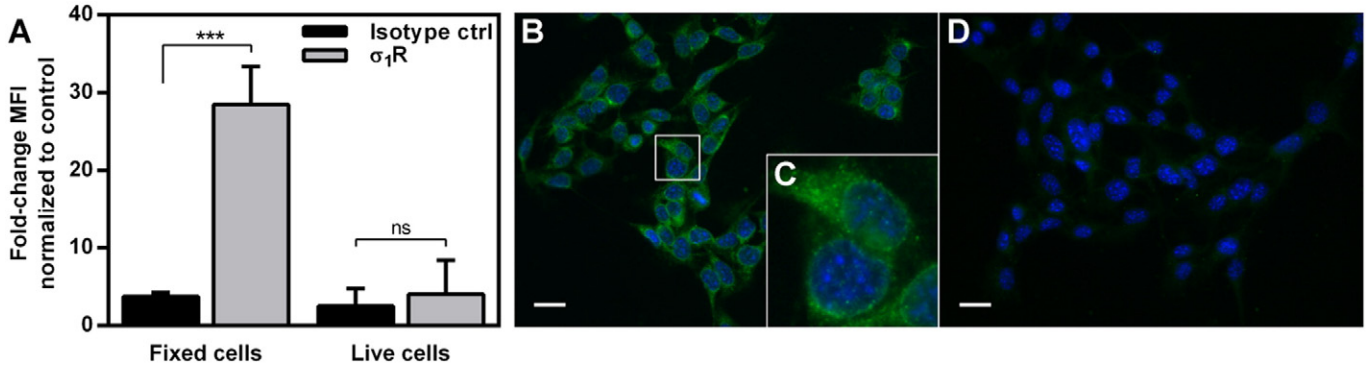

Fig. 5. σ_1R immunostaining on B16-F10 cells. (A) Flow cytometry results of immunostained fixed/permeabilized and live cells with σ_1R antibody or isotype control antibody. MFI values were normalized to those of unstained cells. Results are expressed as mean ± S.D. (n = 3). (ns) $p > 0.05$ and (***) $p < 0.001$ *vs.* indicated bar. (B) Representative fluorescence microscopy image of fixed/permeabilized cells stained with σ_1R antibody. Blue: nucleus, green: σ_1R. (C) Higher magnification of σ_1R-stained cells of the area depicted in (B). (D) Representative fluorescence microscopy image of fixed/permeabilized cells stained with an isotype control antibody. Blue: nucleus, green: IgG isotype control. Scale bars: 25 μm.

numerous examples found in the literature and support the putative selective tumor-targeting potential of the small molecule anisamide when grafted to particles [11,18,21,23–26]. The cell uptake by melanoma cells was, nevertheless, diminished under *in vivo* conditions, which were chosen to promote the interactions between cells and particles. Moreover, the results of this study raised questions concerning the cell target of anisamide. Indeed, our results suggest that the hypothetical anisamide target, the σ_1R, might not be the endocytosis mediator of our anisamide-decorated particles.

A competition uptake experiment with haloperidol co-incubation revealed a non-specific effect of the σ_1R antagonist on endocytosis (Fig. 3C). This finding was supported by a haloperidol-induced uptake reduction of two σ_1R-independent endocytosis markers (Supplementary Fig. S7). The cytotoxicity of the compound may explain this effect. Indeed, cytotoxic effects of haloperidol have been described before, with measured IC_{50} values (concentration of the drug required to reduce cell viability to 50%) around 100 μM after 24 h or 48 h of incubation with the compound and have been attributed to the σ_2R-agonist properties of the drug [40–42]. EC_{50} values (concentration of haloperidol resulting in 50% reduction of the CI value relative to solvent control CI value) in the same concentration range were obtained with the B16-F10 cells used in this study (Supplementary Fig. S12). This cytotoxic effect of haloperidol may be the cause of reduced endocytic activity. In fact, the compound has been found to severely damage the components of the cytoskeleton (which are necessary for the endocytic process) at concentrations in the μM range [43], which in turn might explain the observed alteration of the cellular morphology [44] and decrease in endocytic activity [45] shown by the drug. Cholesterol biosynthesis inhibition, which leads to changes in the plasma membrane composition and could hence influence the endocytic process, has also been reported [46]. These taken into account, the lower cellular uptake of the anisamide-functionalized particles in the presence of haloperidol in this and in previous studies could possibly be attributed to toxicity-related alteration of the endocytic activity of the cells rather than specific effects on σ_1R. No conclusions concerning the interaction of anisamide with σ_1R can, therefore, be drawn from competition experiments with haloperidol.

The prototypical σ_1R agonist (+)-SKF-10,047 [36] did not show competition with the anisamide-decorated particles for σ_1R (Fig. 3C). In addition, our data failed to show any correlation between the expression levels of σ_1R and the extent of uptake of the anisamide-targeted particles. The anisamide-functionalized particles were taken up to the same extent by wild-type and σ_1R-deficient B16-F10 cells (Fig. 4B). Also, 4T1 cells with high levels of σ_1R expression showed low targeted-particle uptake, similar to the uptake observed with non-targeted particles (PS-PEG) (Fig. 4C). Those results indicate that the targeted particle uptake is not proportional to the level of cellular σ_1R expression. Altogether, these data imply that the uptake of the anisamide-tethered particles might not occur *via* the σ_1R.

Finally, the most compelling indication suggesting that σ_1R may not be the main target of anisamide lies with the precise subcellular localization of σ_1R. Active tumor targeting of macromolecules or nanocarriers necessitates direct contact of the targeting ligand on the cell surface for the interaction with tumor cells [7]. Although σ_1R has long been described as a membrane-bound protein [47], the controversies in the literature concerning its subcellular distribution previously hampered the identification of the exact cell loci. Early studies combining subcellular fractionation of homogenized rodent brain tissues with σ_1 ligand binding techniques had proposed the existence of the receptor at the intracellular level, predominantly in the endoplasmic reticulum but also to some extent on the synaptic membrane [48–51]. Two more recent publications claim localization of the receptor on the plasma membrane of a breast cancer cell line [52] and on σ_1R-transfected Xenopus oocytes [53]. On the other hand, examination of the amino acid sequence following the receptor cloning revealed the existence of a putative endoplasmic reticulum retention signal [47,54]. Indeed, by means of more advanced cell biology techniques, it has now been suggested that the protein is intracellular [55]. Immunostaining with σ_1R antibodies has contributed in elucidating the receptor's main cell locus, found in the endoplasmic reticulum [56–60]. The same localization findings are supported by the cell distribution of EYFP-tagged σ_1R transfected in cultured cells [56,60]. Our study using immunostaining techniques clearly demonstrated similar intracellular localization of σ_1R in B16-F10 cells. If this receptor is indeed intracellular, the enhanced *in vivo* tumor uptake of anisamide-decorated nanosystems observed in several previous studies [18,21–26] cannot be attributed to binding of anisamide to σ_1R.

Some molecules belonging to the class of benzamides have been shown to bind σ_2R [61], the other known subtype of the sigma receptor family [62], and this raises the reasonable question whether anisamide also binds to it. One publication describing a 4-methoxybenzamide-targeted nanosystem mentioned that the target of anisamide was σ_2R [27], although the binding to σ_2R was not investigated in that or in any other study. It has been recently demonstrated that σ_2R is implicated in cancer [63], so it might constitute a good target for tumor-directed delivery. However, contrary to σ_1R, σ_2R has not yet been cloned and its sequence remains unknown. Therefore, its tissue expression pattern and subcellular localization are still to be identified. Consequently, while a putative anisamide binding to σ_2R cannot be excluded, it cannot be investigated at the moment, since the available tools for the study of the receptor are limited to *in vitro* binding assays with more or less selective σ_2R ligands [63].

5. Conclusions

The data presented herein suggest that the high uptake by B16-F10 melanoma cells of the anisamide-decorated particles of our work might not occur *via* σ_1R. Nevertheless, the effect of the particle size on uptake should not be overlooked. The particles studied in this work are larger than the anisamide-functionalized nanoparticles reported in the literature and one could argue that a size of 1-μm diameter might be too large for internalization by receptor-mediated endocytosis (although we clearly observed a difference in uptake between the melanoma cells and the macrophages). A size-effect study would, therefore, be necessary before we generalize our conclusions to all the anisamide-decorated systems. However, our attempt to reproduce the cell uptake results with liposomes of 200-nm diameter led to merely low increase of uptake. An extensive study of anisamide-tethered nanosized particles would be necessary to fully elucidate the mechanism of endocytosis in future studies.

Nevertheless, our results from experiments not involving particles also raise serious doubts regarding the interaction of anisamide with σ_1R. Firstly, information derived from the competition uptake assay with haloperidol (the only type of experiment employed in preceding reports on which the hypothesis of Sigma-1 receptor binding was based) from the literature appears to be unreliable, as we have shown that the reported observations were probably due to toxic effects of the compound on the cells. In addition, the evidence we provide in this work concerning the intracellular localization of σ_1R, which is in line with the recent literature, goes against the possibility of use of σ_1R as a target for tumor-directed nanocarriers.

If this previously suggested hypothesis of σ_1R-mediated endocytosis is indeed not valid, the mechanism of cellular uptake of anisamide-decorated nanocarriers still needs to be elucidated. It will be worth investigating if the interactions of anisamide with tumor cells are really selective, with σ_2R as an example of a possible tumor-cell target, or if the effect of high uptake is non-selective, induced for instance by alteration of the physicochemical properties of the particles caused by the presence of ligand on the surface. The complete knowledge of how anisamide enhances the endocytosis of nanocarriers will be of great significance for the full exploitation of its putative tumor targeting properties.

Acknowledgments

The authors kindly thank the Scientific Center for Optical and Electron Microscopy (ScopeM) of ETH Zurich for use of the facility, and especially Joachim Hehl for assistance with confocal laser scanning microscopy and Dr. Miriam Lucas for the TEM. The ETH Zurich Flow Cytometry facility is acknowledged for assistance with the LSRFortessa cytometer measurements. Dr. Maija Hollmén, Dr. Davide Brambilla and Xiangang Huang are warmly thanked for scientific support. Funding by Krebsliga Schweiz (KFS-2821-08-2011) is gratefully acknowledged.

Appendix A. Supplementary data

Supplementary data to this article can be found online at http://dx.doi.org/10.1016/j.jconrel.2016.01.021.

References

[1] D. Hanahan, R.A. Weinberg, Hallmarks of cancer: the next generation, Cell 144 (2011) 646–674, http://dx.doi.org/10.1016/j.cell.2011.02.013.
[2] T. Sun, Y.S. Zhang, B. Pang, D.C. Hyun, M. Yang, Y. Xia, Engineered nanoparticles for drug delivery in cancer therapy, Angew. Chem. Int. Ed. Engl. 53 (2014) 12320–12364, http://dx.doi.org/10.1002/anie.201403036.
[3] Time to deliver, Nat. Biotechnol. 32 (2014) 961, http://dx.doi.org/10.1038/nbt.3045.
[4] D. Brambilla, P. Luciani, J.-C. Leroux, Breakthrough discoveries in drug delivery technologies: the next 30 years, J. Control. Release 190 (2014) 9–14, http://dx.doi.org/10.1016/j.jconrel.2014.03.056.
[5] J.D. Byrne, T. Betancourt, L. Brannon-Peppas, Active targeting schemes for nanoparticle systems in cancer therapeutics, Adv. Drug Deliv. Rev. 60 (2008) 1615–1626, http://dx.doi.org/10.1016/j.addr.2008.08.005.
[6] Y. Zhong, F. Meng, C. Deng, Z. Zhong, Ligand-directed active tumor-targeting polymeric nanoparticles for cancer chemotherapy, Biomacromolecules 15 (2014) 1955–1969, http://dx.doi.org/10.1021/bm5003009.
[7] N. Bertrand, J. Wu, X. Xu, N. Kamaly, O.C. Farokhzad, Cancer nanotechnology: the impact of passive and active targeting in the era of modern cancer biology, Adv. Drug Deliv. Rev. 66 (2014) 2–25, http://dx.doi.org/10.1016/j.addr.2013.11.009.
[8] J.R. McCarthy, R. Weissleder, Multifunctional magnetic nanoparticles for targeted imaging and therapy, Adv. Drug Deliv. Rev. 60 (2008) 1241–1251, http://dx.doi.org/10.1016/j.addr.2008.03.014.
[9] Y. Lu, P.S. Low, Folate-mediated delivery of macromolecular anticancer therapeutic agents, Adv. Drug Deliv. Rev. 64 (2012) 342–352, http://dx.doi.org/10.1016/j.addr.2012.09.020.
[10] J. Hrkach, D. Von Hoff, M. Mukkaram Ali, E. Andrianova, J. Auer, T. Campbell, et al., Preclinical development and clinical translation of a PSMA-targeted docetaxel nanoparticle with a differentiated pharmacological profile, Sci. Transl. Med. 4 (2012) 128ra39, http://dx.doi.org/10.1126/scitranslmed.3003651.
[11] R. Banerjee, P. Tyagi, S. Li, L. Huang, Anisamide-targeted stealth liposomes: a potent carrier for targeting doxorubicin to human prostate cancer cells, Int. J. Cancer 112 (2004) 693–700, http://dx.doi.org/10.1002/ijc.20452.
[12] C.S. John, B.J. Vilner, B.C. Geyer, T. Moody, W.D. Bowen, Targeting sigma receptor-binding benzamides as in vivo diagnostic and therapeutic agents for human prostate tumors, Cancer Res. 59 (1999) 4578–4583.
[13] C.S. John, W.D. Bowen, S.J. Fisher, B.B. Lim, B.C. Geyer, B.J. Vilner, et al., Synthesis, in vitro pharmacologic characterization, and preclinical evaluation of N-[2-(1′-Piperidinyl)ethyl]-3-[125I]iodo-4-methoxybenzamide (P[125I]MBA) for imaging breast cancer, Nucl. Med. Biol. 26 (1999) 377–382, http://dx.doi.org/10.1016/S0969-8051(98)00104-8.
[14] V. Megalizzi, M. Le Mercier, C. Decaestecker, Sigma receptors and their ligands in cancer biology: overview and new perspectives for cancer therapy, Med. Res. Rev. 32 (2010) 410–427, http://dx.doi.org/10.1002/med.
[15] E. Aydar, C.P. Palmer, M.B.A. Djamgoz, Sigma receptors and cancer: possible involvement of ion channels, Cancer Res. 64 (2004) 5029–5035, http://dx.doi.org/10.1158/0008-5472.CAN-03-2329.
[16] B.J. Vilner, C.S. John, W.D. Bowen, Sigma-1 and sigma-2 receptors are expressed in a wide variety of human and rodent tumor cell lines, Cancer Res. 55 (1995) 408–413.
[17] N. Mackiewicz, J. Nicolas, N. Handké, M. Noiray, J. Mougin, C. Daveu, et al., Precise engineering of multifunctional PEGylated polyester nanoparticles for cancer cell targeting and imaging, Chem. Mater. 26 (2014) 1834–1847, http://dx.doi.org/10.1021/cm403822w.
[18] J. Guo, J.R. Ogier, S. Desgranges, R. Darcy, C. O'Driscoll, Anisamide-targeted cyclodextrin nanoparticles for siRNA delivery to prostate tumours in mice, Biomaterials 33 (2012) 7775–7784, http://dx.doi.org/10.1016/j.biomaterials.2012.07.012.
[19] Y. Zhang, W.Y. Kim, L. Huang, Systemic delivery of gemcitabine triphosphate via LCP nanoparticles for NSCLC and pancreatic cancer therapy, Biomaterials 34 (2013) 3447–3458, http://dx.doi.org/10.1016/j.biomaterials.2013.01.063.
[20] J.L. Vivero-Escoto, K.M.L. Taylor-Pashow, R.C. Huxford, J. Della Rocca, C. Okoruwa, H. An, et al., Multifunctional mesoporous silica nanospheres with cleavable Gd(III) chelates as MRI contrast agents: synthesis, characterization, target-specificity, and renal clearance, Small 7 (2011) 3519–3528, http://dx.doi.org/10.1002/smll.201100521.
[21] B.L. Rodriguez, J.M. Blando, D.S.P. Lansakara-P, Y. Kiguchi, J. DiGiovanni, Z. Cui, Antitumor activity of tumor-targeted RNA replicase-based plasmid that expresses interleukin-2 in a murine melanoma model, Mol. Pharm. 10 (2013) 2404–2415, http://dx.doi.org/10.1021/mp400033m.
[22] S.K. Kim, L. Huang, Nanoparticle delivery of a peptide targeting EGFR signaling, J. Control. Release 157 (2012) 279–286, http://dx.doi.org/10.1016/j.jconrel.2011.08.014.
[23] S.K. Kim, M.B. Foote, L. Huang, Targeted delivery of EV peptide to tumor cell cytoplasm using lipid coated calcium carbonate nanoparticles, Cancer Lett. 334 (2013) 311–318, http://dx.doi.org/10.1016/j.canlet.2012.07.011.
[24] Y. Yang, Y. Hu, Y. Wang, J. Li, F. Liu, L. Huang, Nanoparticle delivery of pooled siRNA for effective treatment of non-small cell lung cancer, Mol. Pharm. (2012)http://dx.doi.org/10.1021/mp300152v.
[25] J. Li, Y.-C. Chen, Y.-C. Tseng, S. Mozumdar, L. Huang, Biodegradable calcium phosphate nanoparticle with lipid coating for systemic siRNA delivery, J. Control. Release 142 (2010) 416–421, http://dx.doi.org/10.1016/j.jconrel.2009.11.008.
[26] J. Yao, Y. Zhang, S. Ramishetti, Y. Wang, L. Huang, Turning an antiviral into an anticancer drug: nanoparticle delivery of acyclovir monophosphate, J. Control. Release 170 (2013) 414–420, http://dx.doi.org/10.1016/j.jconrel.2013.06.009.
[27] H. He, A.W. Cattran, T. Nguyen, A.-L. Nieminen, P. Xu, Triple-responsive expansile nanogel for tumor and mitochondria targeted photosensitizer delivery, Biomaterials 35 (2014) 9546–9553, http://dx.doi.org/10.1016/j.biomaterials.2014.08.004.
[28] O. Nakagawa, X. Ming, L. Huang, R.L. Juliano, Targeted intracellular delivery of antisense oligonucleotides via conjugation with small-molecule ligands, J. Am. Chem. Soc. 132 (2010) 8848–8849, http://dx.doi.org/10.1021/ja102635c.
[29] S. Guo, C.M. Lin, Z. Xu, L. Miao, Y. Wang, L. Huang, Co-delivery of cisplatin and rapamycin for enhanced anticancer therapy through synergistic effects and microenvironment modulation, ACS Nano 8 (2014) 4996–5009, http://dx.doi.org/10.1021/nn5010815.
[30] S.T. Proulx, P. Luciani, A. Christiansen, S. Karaman, K.S. Blum, M. Rinderknecht, et al., Use of a PEG-conjugated bright near-infrared dye for functional imaging of rerouting of tumor lymphatic drainage after sentinel lymph node metastasis, Biomaterials 34 (2013) 5128–5137, http://dx.doi.org/10.1016/j.biomaterials.2013.03.034.
[31] E. Urcan, U. Haertel, M. Styllou, R. Hickel, H. Scherthan, F.X. Reichl, Real-time xCELLigence impedance analysis of the cytotoxicity of dental composite components on human gingival fibroblasts, Dent. Mater. 26 (2010) 51–58, http://dx.doi.org/10.1016/j.dental.2009.08.007.
[32] S.-D. Li, S. Chono, L. Huang, Efficient gene silencing in metastatic tumor by siRNA formulated in surface-modified nanoparticles, J. Control. Release 126 (2008) 77–84, http://dx.doi.org/10.1016/j.jconrel.2007.11.002.
[33] Z. Xu, Y. Wang, L. Zhang, L. Huang, Nanoparticle-delivered transforming growth factor-β siRNA enhances vaccination against advanced melanoma by modifying tumor microenvironment, ACS Nano 8 (2015) 3636–3645, http://dx.doi.org/10.1021/nn500216y.
[34] S. Chono, S.-D. Li, C.C. Conwell, L. Huang, An efficient and low immunostimulatory nanoparticle formulation for systemic siRNA delivery to the tumor, J. Control. Release 131 (2008) 64–69, http://dx.doi.org/10.1016/j.jconrel.2008.07.006.
[35] Y. Zhang, N.M. Schwerbrock, A.B. Rogers, W.Y. Kim, L. Huang, Codelivery of VEGF siRNA and gemcitabine monophosphate in a single nanoparticle formulation for effective treatment of NSCLC, Mol. Ther. 21 (2013) 1559–1569, http://dx.doi.org/10.1038/mt.2013.120.
[36] E.J. Cobos, J.M. Entrena, F.R. Nieto, C.M. Cendán, E. Del Pozo, Pharmacology and therapeutic potential of sigma1 receptor ligands, Curr. Neuropharmacol. 6 (2008) 344–366, http://dx.doi.org/10.2174/157015908787386113.
[37] S. Falcone, E. Cocucci, P. Podini, T. Kirchhausen, E. Clementi, J. Meldolesi, Macropinocytosis: regulated coordination of endocytic and exocytic membrane traffic events, J. Cell Sci. 119 (2006) 4758–4769, http://dx.doi.org/10.1242/jcs.03238.
[38] D. Vercauteren, R.E. Vandenbroucke, A.T. Jones, J. Rejman, J. Demeester, S.C. De Smedt, et al., The use of inhibitors to study endocytic pathways of gene carriers: optimization and pitfalls, Mol. Ther. 18 (2010) 561–569, http://dx.doi.org/10.1038/mt.2009.281.
[39] J.A.E.S. Kang, D. Cho, Y. Kim, E. Hahm, Y.S. Kim, S.N.U. Jin, et al., Sodium ascorbate (vitamin C) induces apoptosis in melanoma cells via the down-regulation of transferrin receptor dependent iron uptake, J. Cell. Physiol. 204 (2005) 192–197, http://dx.doi.org/10.1002/jcp.20286.
[40] Z. Wei, D.D. Mousseau, Y. Dai, X. Cao, X.-M. Li, Haloperidol induces apoptosis via the sigma2 receptor system and Bcl-XS, Pharmacogenomics J. 6 (2006) 279–288, http://dx.doi.org/10.1038/sj.tpj.6500373.
[41] A.A. Rybczynska, R.A. Dierckx, K. Ishiwata, P.H. Elsinga, A. van Waarde, Cytotoxicity of sigma-receptor ligands is associated with major changes of cellular metabolism and complete occupancy of the sigma-2 subpopulation, J. Nucl. Med. 49 (2008) 2049–2056, http://dx.doi.org/10.2967/jnumed.108.053876.
[42] Z. Wei, J. Qi, Y. Dai, W.D. Bowen, D.D. Mousseau, Haloperidol disrupts Akt signalling to reveal a phosphorylation-dependent regulation of pro-apoptotic Bcl-XS function, Cell. Signal. 21 (2009) 161–168, http://dx.doi.org/10.1016/j.cellsig.2008.10.005.
[43] G. Benítez-King, L. Ortíz-López, G. Jiménez-Rubio, G. Ramírez-Rodríguez, Haloperidol causes cytoskeletal collapse in N1E-115 cells through tau hyperphosphorylation induced by oxidative stress: implications for neurodevelopment, Eur. J. Pharmacol. 644 (2010) 24–31, http://dx.doi.org/10.1016/j.ejphar.2010.06.057.
[44] B.J. Vilner, F. De Costa, D. Bowen, Cytotoxic effects of sigma ligands: sigma receptor-mediated alterations in cellular morphology and viability, J. Neurosci. 15 (1995) 117–134.
[45] M.-L. Chen, S. Wu, T.-C. Tsai, L.-K. Wang, F.-M. Tsai, Regulation of macrophage immune responses by antipsychotic drugs, Immunopharmacol. Immunotoxicol. 35 (2013) 573–580, http://dx.doi.org/10.3109/08923973.2013.828744.

[46] J. Sánchez-Wandelmer, A. Dávalos, G. de la Peña, S. Cano, M. Giera, A. Canfrán-Duque, et al., Haloperidol disrupts lipid rafts and impairs insulin signaling in SH-SY5Y cells, Neuroscience 167 (2010) 143–153, http://dx.doi.org/10.1016/j.neuroscience.2010.01.051.
[47] M. Hanner, F.F. Moebius, A. Flandorfer, H.G. Knaus, J. Striessnig, E. Kempner, et al., Purification, molecular cloning, and expression of the mammalian sigma1-binding site, Proc. Natl. Acad. Sci. U. S. A. 93 (1996) 8072–8077.
[48] Y. Itzhak, I. Stein, S. Zhang, C.O. Kassim, D. Cristante, Binding of σ-ligands to C57BL/6 mouse brain membranes: effects of monoamine oxidase inhibitors and subcellular distribution studies suggest the existence of σ-receptor subtypes, J. Pharmacol. Exp. Ther. 257 (1991) 141–148.
[49] A. Cagnotto, A. Bastone, T. Mennini, [3H](+)-pentazocine binding to rat brain sigma 1 receptors, Eur. J. Pharmacol. 266 (1994) 131–138, http://dx.doi.org/10.1016/0922–4106(94)90102–3.
[50] D.L. DeHaven-Hudkins, L.F. Lanyon, F.Y. Ford-Rice, M.A. Ator, σ recognition sites in brain and peripheral tissues — characterization and effects of cytochrome P450 inhibitors, Biochem. Pharmacol. 47 (1994) 1231–1239, http://dx.doi.org/10.1016/0006–2952(94)90395–6.
[51] E.J. Cobos, E. del Pozo, J.M. Baeyens, Irreversible blockade of sigma-1 receptors by haloperidol and its metabolites in guinea pig brain and SH-SY5Y human neuroblastoma cells, J. Neurochem. 102 (2007) 812–825, http://dx.doi.org/10.1111/j.1471-4159.2007.04533.x.
[52] E. Aydar, P. Onganer, R. Perrett, M.B. Djamgoz, C.P. Palmer, The expression and functional characterization of sigma (σ) 1 receptors in breast cancer cell lines, Cancer Lett. 242 (2006) 245–257, http://dx.doi.org/10.1016/j.canlet.2005.11.011.
[53] E. Aydar, C.P. Palmer, V.A. Klyachko, M.B. Jackson, The sigma receptor as a ligand-regulated auxiliary potassium channel subunit, Neuron 34 (2002) 399–410, http://dx.doi.org/10.1016/S0896-6273(02)00677–3.
[54] R. Kekuda, P.D. Prasad, Y. Fei, F.H. Leibach, V. Ganapathy, Cloning and functional expression of the human type 1 sigma receptor (hSigmaR1), Biochem. Biophys. Res. Commun. 229 (1996) 553–558, http://dx.doi.org/10.1006/bbrc.1996.1842.
[55] T. Hayashi, T.-P. Su, Subcellular localization and intracellular dynamics of σ1 receptors, in: R.R. Matsumoto, W.D. Bowen, T.-P. Su (Eds.), Sigma Recept. Chem. Cell Biol. Clin. Implic. Springer Science, New York 2007, pp. 151–164.
[56] T. Hayashi, T.-P. Su, σ-1 receptors (σ1 binding sites) form raft-like microdomains and target lipid droplets on the endoplasmic reticulum: roles in endoplasmic reticulum lipid compartmentalization and export, J. Pharmacol. Exp. Ther. 306 (2003) 718–725, http://dx.doi.org/10.1124/jpet.103.051284.
[57] T. Hayashi, T. Su, Regulating ankyrin dynamics: roles of sigma-1 receptors, Proc. Natl. Acad. Sci. U. S. A. 98 (2001) 491–496, http://dx.doi.org/10.1073/pnas.98.2.491.
[58] M. Esslimani, E. Bribes, S. Gourgou, N. Lequeux, R. Lavail, J. Grenier, et al., Immunocytochemical assessment of sigma-1 receptor and human sterol isomerase in breast cancer and their relationship with a series of prognostic factors, Br. J. Cancer 82 (2000) 1958–1966, http://dx.doi.org/10.1054/bjoc.2000.1162.
[59] D. Dussossoy, P. Carayon, S. Belugou, D. Feraut, A. Bord, C. Goubet, et al., Colocalization of sterol isomerase and sigma 1 receptor at endoplasmic reticulum and nuclear envelope level, Eur. J. Biochem. 263 (1999) 377–385, http://dx.doi.org/10.1046/j.1432-1327.1999.00500.x.
[60] T. Hayashi, T.-P. Su, Intracellular dynamics of σ-1 receptors (σ1 binding sites) in NG108-15 cells, J. Pharmacol. Exp. Ther. 306 (2003) 726–733, http://dx.doi.org/10.1124/jpet.103.051292.
[61] Y.-S. Huang, H.-L. Lu, L.-J. Zhang, Z. Wu, Sigma-2 receptor ligands and their perspectives in cancer diagnosis and therapy, Med. Res. Rev. 34 (2014) 532–566, http://dx.doi.org/10.1002/med.21297.
[62] R.R. Matsumoto, σ receptors: historical perspective and background, in: R.R. Matsumoto, W.D. Bowen, T. Su (Eds.), Sigma Recept. Chem. Cell Biol. Clin. Implic. Springer 2007, pp. 1–23.
[63] R.H. Mach, C. Zeng, W.G. Hawkins, The σ2 receptor: a novel protein for the imaging and treatment of cancer, J. Med. Chem. 56 (2012) 7137–7160, http://dx.doi.org/10.1021/jm301545c.